JOURNAL OF MATERIALS SCIENCE **40** (2005) 63–70

Electrical and elastic properties of new monolithic wood-based carbon materials

A. CELZARD*
Laboratoire de Chimie du Solide Minéral, Université Henri Poincaré - Nancy I, UMR - CNRS 7555, BP 239, 54506 Vandoeuvre-lès-Nancy, France
E-mail: Alain.Celzard@lcsm.uhp-nancy.fr

O. TREUSCH
Technische Universität München, Holzforschung München,Winzererstr. 45, 80797 München, Germany

J. F. MARÊCHÉ
Laboratoire de Chimie du Solide Minéral, Université Henri Poincaré - Nancy I, UMR - CNRS 7555, BP 239, 54506 Vandoeuvre-lès-Nancy, France

G. WEGENER
Technische Universität München, Holzforschung München,Winzererstr. 45, 80797 München, Germany

Carbonaceous monolithic materials were prepared from especially designed wood-based composites consisting of wood fibres and phenolic resin binder. By compressing more or less the starting materials, the monoliths were obtained with densities ranging from 0.3 to 1.2 g cm^{-3}. After carbonisation, electrical conductivity and elastic moduli of a number of samples were investigated, and typical percolation behaviours were evidenced for both properties close to their respective critical points. Careful study of the apparent density and pore texture of the uncompacted carbonised fibres allowed the determination of the conductivity threshold Φ_c. The morphologies of both the constitutive carbon particles and the interparticle voids were derived from application of effective-medium theory; the calculated aspect ratio of the fibres was found to be in good agreement with both SEM characterisations and other calculations based on percolation theory. Observation of the universal 3D value of the critical conductivity exponent supported the accuracy of the estimated value of Φ_c. The rigidity threshold Φ_r was also determined, and the relevance of the Kirkwood-Keating model accounting for the observed relationship between Φ_c and Φ_r was established. The value of the elasticity critical exponent suggested central forces between the fibres, further supporting the suitability of the Kirkwood-Keating model. To the knowledge of the authors, such a model was shown to apply to only one other material so far: expanded graphite. Hence, the present work shows the relevance of the classical concepts of disordered matter physics for describing heterogeneous random carbonaceous materials.

1. Introduction

Percolation and effective-medium theories (PT and EMT, respectively) are actually known to be very powerful tools of investigating various phenomena in heterogeneous materials. Lists and examples of their applications may be found in a number of review articles and monographs [1–5]. If the shape of randomly dispersed objects is known, PT predicts both the position of the connectivity threshold (i.e., the critical volume fraction of objects at which a connection is established all through the system) and the behaviour of some physical properties of the disordered system close to this threshold. Conversely, quantitative information about the morphology of the percolating objects may be derived from the value of their critical volume fraction. Additionally, through the critical behaviour observed near the percolation threshold, the nature of the contacts between the objects may be specified. EMT may bring the same kind of information, but applies to a larger class of disordered systems, having wide ranges of compositions and sometimes not exhibiting any percolation threshold. Anyway, percolation laws

*Author to whom all correspondence should be addressed.

may often be derived from limiting forms of equations based on EMT. Hence, PT and EMT either lead to similar results or are highly complementary with each other.

Both theories were already applied to a large number of different model materials, mainly for confirming theoretical predictions. Recently, it was shown that the physical properties of many carbonaceous materials were accurately accounted for by PT and EMT, and that very important structural information could be derived from their application. Especially, composite materials based on dispersed graphite flakes of carbon fibres [6], carbonised anthracites [7], carbon powders [8, 9] and compressed expanded graphite [10–13] were suitably described through these two theories. Indeed, most carbonaceous materials are made of particles, either dense or porous, having typical well-defined shapes, ranging from spheres to flakes, platelets and needles, passing by oblate or prolate ellipsoids. Besides, observations show that such morphologies are very homogeneous within a given batch of particles. Hence, many carbonaceous materials are useful disordered model systems for applying both PT and EMT.

In the present work, new monolithic carbonaceous wood-based materials were investigated. The preparation of these materials is first described and their main features (microstructure, chemical composition, pore volume and surface area) are given in Section 2. Electrical conductivity and elastic modulus are then measured and the results are discussed in Section 3. Finally, the morphological characteristics of both the solid and the pore phases are derived, and several theoretical considerations are also developed.

2. Materials

2.1. Preparation of monolithic carbonaceous wood-based materials

Wood-based composites were made by mixing wood fibres with 10% of a powdery phenolic resin (Bakelite) in a stirring device. Subsequently the mixture was pressed to form boards of 10 mm thickness and densities from 0.3 to 1.2 g cm^{-3} in a uni-axial pressing process at a temperature of 180°C. The fibreboards were dried at 103°C for 2 h, and their carbonisation was carried out using specimens sized 600 mm × 800 mm, in an inert atmosphere (N_2). To make sure that the carbon materials remained crack-free, a slow heating rate of 1 K/min was applied up to 500°C. A heating rate of 5 K/min was applied up to the peak temperature of 900°C, which was kept for 2 h.

2.2. Main features of the monolithic materials

Due to their rather high heat-treatment temperature (900°C), the materials are made of almost pure carbon. Elemental analysis (Heraeus CHN-O-RAPID) leads to the following elemental massic composition: C 98%, H 0.5%, O 1.5%. From the point of view of their physical properties, the present monoliths are then expected to behave like rigid electrically conducting carbon "sponges".

As seen by SEM pictures like that presented in Fig. 1, the fibre-like particles within the monolithic materials are randomly disordered and entangled with each other. In agreement with such a microstructure, the monoliths are, macroscopically speaking, perfectly homogeneous and exhibit no anisotropy. Additionally, they are crack-free, thus allowing the measurement of both their conducting and elastic properties.

With the aim of characterising them accurately, a sample of uncompacted wood fibres was pyrolized in the same conditions as those already used for the monoliths (i.e., up to 900°C according to the heating rate detailed above). Fig. 2 shows the wood fibres (a) before and (b) after carbonisation. According to the supplier, the crude wood fibres should have diameters of about 30 μm and lengths ranging typically from 400 to 500 μm, leading to ratios length to diameter within the range 13–17. Fig. 2a shows that, even if such high aspect ratios may sometimes be found, most of the particles are shorter, which lengths being typically slightly below 300 μm. On the other hand, their average diameter is really close to 30 μm. Carbonising the fibres does not seem to have much effect on their morphology, since Fig. 2b is very similar to Fig. 2a. Measuring the dimensions of a number of particles leads to an average ratio length to diameter close to 10. After carbonisation, the fine resulting powder was studied via nitrogen adsorption at 77 K and by mercury porosimetry. The apparent density of the uncompacted pyrolized material is $d_p \approx 9.5 \times 10^{-2}$ g cm^{-3}, and the measured BET surface area is 515 m^2 g^{-1}. The micropore volume (corresponding to pore sizes < 2 nm) was estimated at 0.2 cm^3 g^{-1}, while the mesopore volume (2–50 nm pore width) was found to be 0.02 cm^3 g^{-1}. Mercury intrusion porosimetry could evidence only very large macropores, which were consequently completely ascribed to interparticle voids. Thus, the constituting particles were assumed to be carbon fibres having a total pore volume $V_p = 0.22$ cm^3 g^{-1}. The bulk density of the carbonaceous backbone of such fibres was measured by helium pycnometry, and the same value of $d_b = 2.0$ g cm^{-3} was always recovered, whatever the density of the monolithic materials. Hence, the apparent density d_{wf} of a typical carbonised wood fibre could be calculated according to:

$$d_{wf} = \frac{1}{V_p + \frac{1}{d_b}}. \quad (1)$$

Then, given the above data for V_p and d_b, $d_{wf} \approx 1.39$ g cm^{-3}. Knowing such a value is very important since the volume fraction Φ of fibres, i.e., of solid grains, within the monoliths having various densities may now be derived. Indeed, the volumic particle content is calculated as:

$$\Phi = \frac{d}{d_{wf}}, \quad (2)$$

where d is the density of each monolithic material.

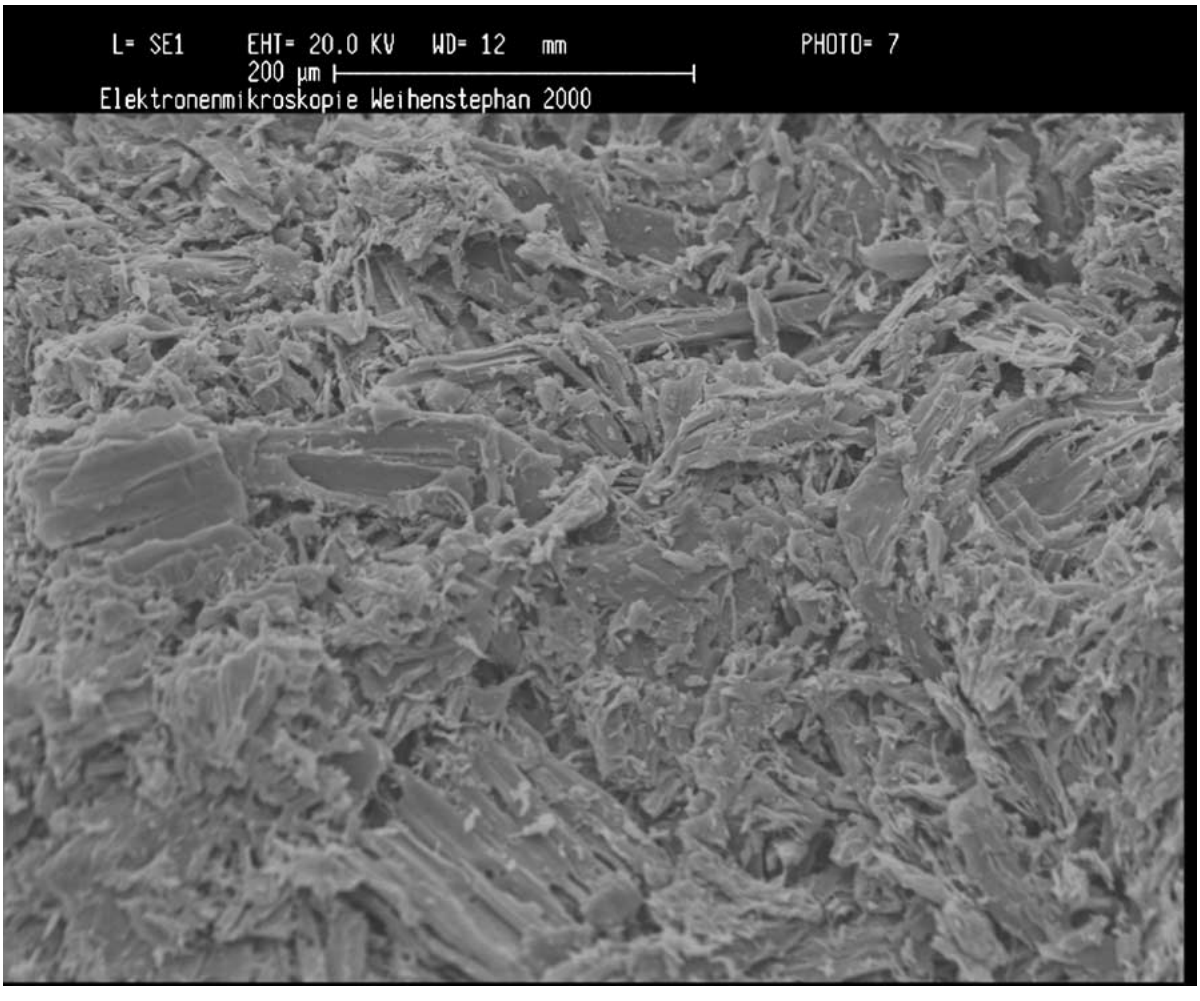

Figure 1 Scanning Electron Microscope (SEM) picture of a wood-based monolith having a density of 0.67 g cm^{-3}.

3. Physical properties of the monoliths

3.1. Electrical conductivities

Parallelepipedic samples, having typical sizes 3 × 1 × 0.5 cm, were cut. The smallest opposite faces were covered with silver paint, with which two copper wires were glued to each surface. The electrical conductivity was then measured according to the 4-probe method, applying low currents so as to avoid Joule heating. By changing the direction of the applied current and taking the arithmetic mean of the two corresponding voltage drops, the measurements were corrected from very low thermo-electric contributions.

The conductivity of the monoliths, σ_m, plotted versus the volume fraction Φ of conducting grains within the monoliths is presented in Fig. 3. The plot clearly shows the existence of a non-zero critical content Φ_c, i.e., a percolation threshold, at which σ_m vanishes. Above but near Φ_c, PT predicts that the conductivity reads [1–3]:

$$\sigma_m = \sigma_h(\Phi - \Phi_c)^t. \quad (3)$$

In Equation 3, Φ is the volume fraction of the high-conductivity phase (here, the carbon fibre-like particles), Φ_c the critical volume fraction at which such particles first percolate, σ_h is the intrinsic conductivity of the latter, and t is the percolation conductivity critical exponent. For classical three-dimensional systems, the value of t is usually close to 2 [1, 14].

The curves $\sigma_m(\Phi)$ may also be studied in the framework of EMT, for which each grain of a binary mixture is surrounded by an average medium possessing the effective conductivity of the composite material itself. A formula able to describe a binary disordered medium in which neither the grains of the two phases are mixed together on a symmetric basis, nor one phase completely coats the other, has been proposed by McLachlan [15, 16] and is known as the general effective media (GEM) equation. It may be written as:

$$(1-\Phi)\frac{\Sigma_l - \Sigma_m}{\Sigma_l + \frac{1-\Phi_c}{\Phi_c}\Sigma_m} + \Phi\frac{\Sigma_h - \Sigma_m}{\Sigma_h + \frac{1-\Phi_c}{\Phi_c}\Sigma_m} = 0 \quad (4)$$

where the constituting terms are defined below.

$$\begin{cases} \Sigma_m = \sigma_m^{1/t'}; & \sigma_m = \text{conductivity of the composite medium (monolith)} \\ \Sigma_l = \sigma_l^{1/t'}; & \sigma_l = \text{conductivity of the low-conductivity phase (air)} \\ \Sigma_h = \sigma_h^{1/t'}; & \sigma_h = \text{conductivity of the high-conductivity phase (carbon)} \end{cases} \quad (5)$$

t' is an exponent related both to the critical volume fraction Φ_c and to the shape of the grains. It may be noticed that modified forms of Equations 4–5 have been

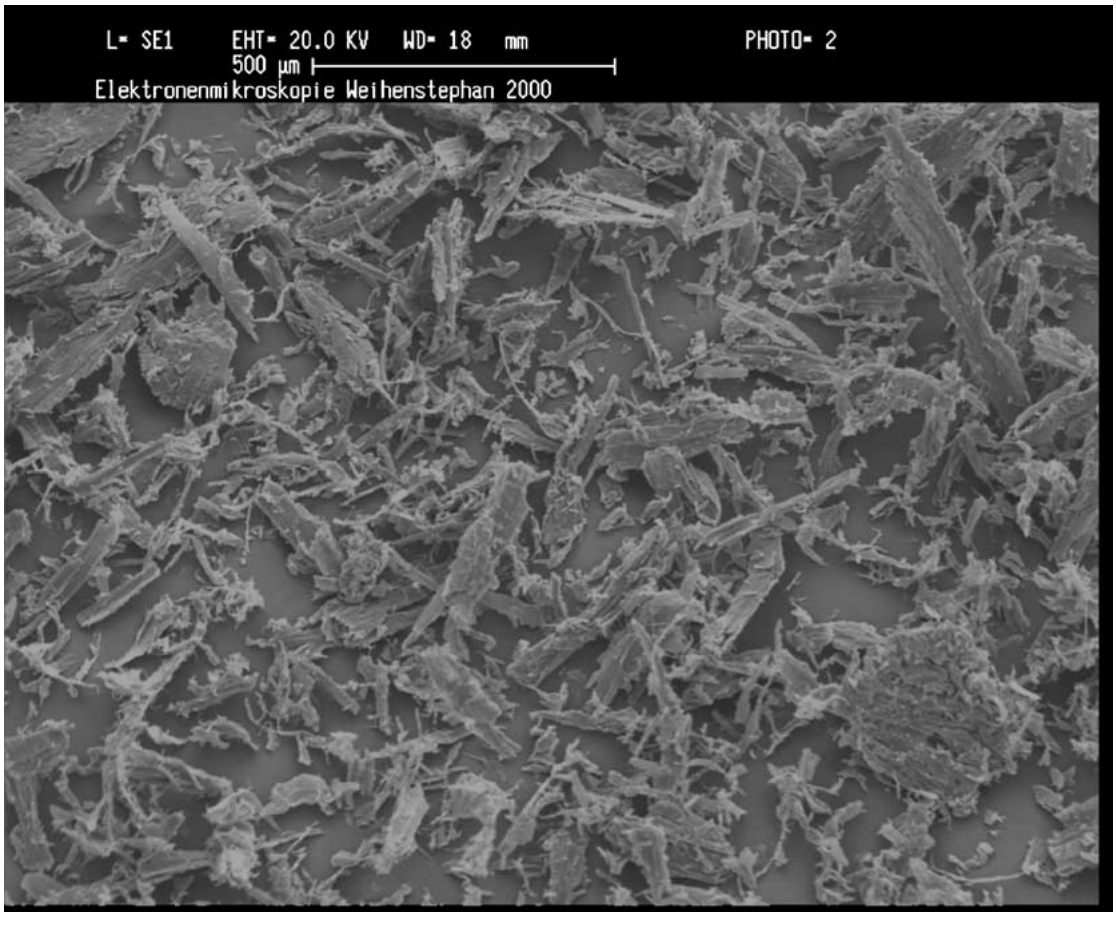

(a)

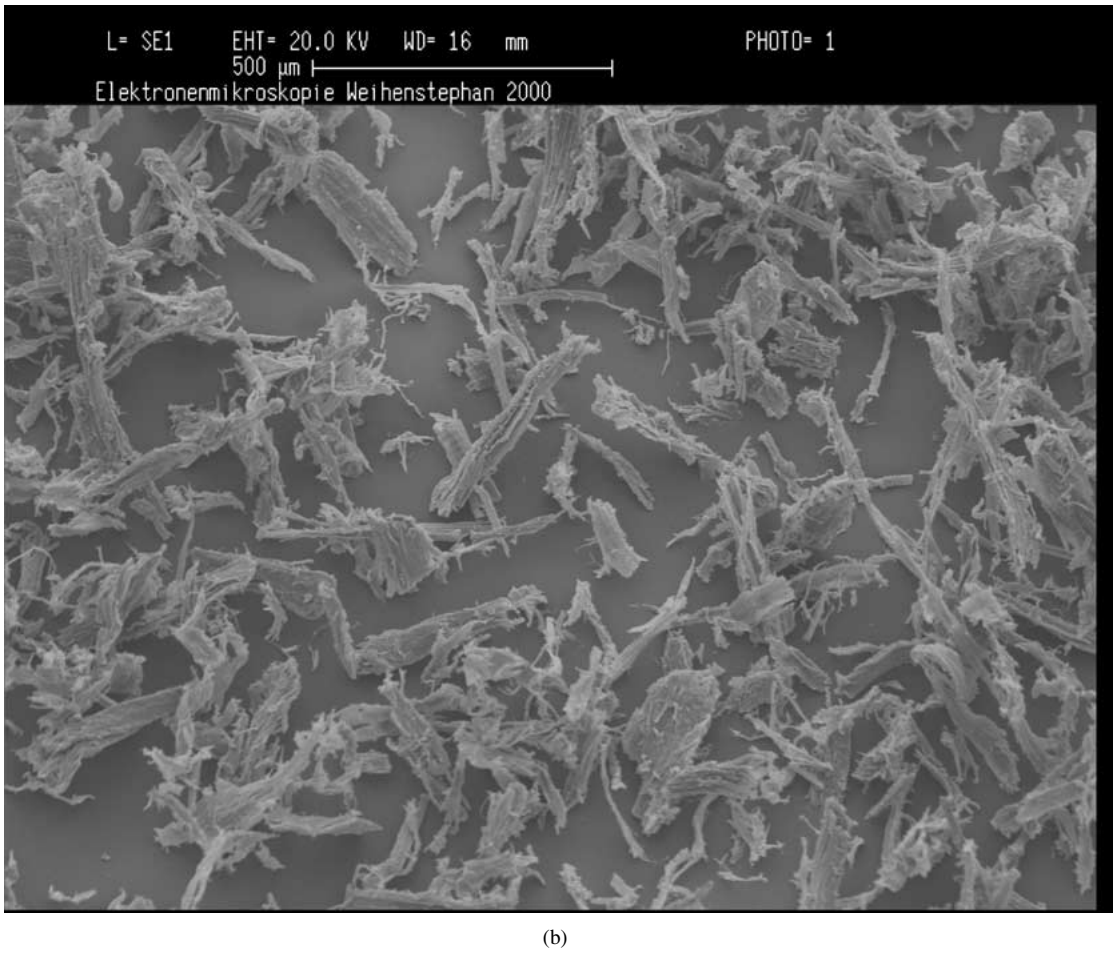

(b)

Figure 2 SEM picture of (a) the crude and (b) the carbonised wood fibres. Measuring the dimensions of a number of particles, the average ratio length to diameter is found to be close to 10 for both pictures.

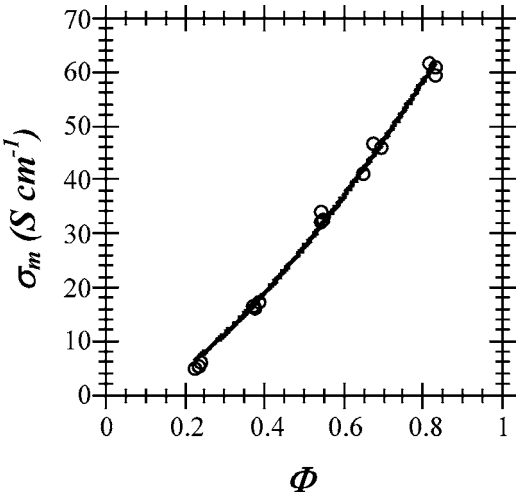

Figure 3 Electrical conductivity (σ_m) of the wood-based monoliths as a function of their volume fraction (Φ) of carbon particles. The solid curve is the fit of the EMT-derived Equation 6 to the experimental data points.

suggested [17, 18] in order to fit more accurately the experimental data below the percolation threshold. However, the present study is only concerned with materials having volume fractions of conducting phase well above the critical content. Besides, in the case of porous monoliths, i.e., mixtures of conducting grains and air, $\sigma_l = 0$ and hence Equations 4–5 and their possible modified forms always reduce to:

$$\sigma_m = \sigma_h \left(\frac{\Phi - \Phi_c}{1 - \Phi_c} \right)^{t'} . \tag{6}$$

This formula has the same form as the percolation Equation 3. Nevertheless, while the percolation exponent t was only expected to take universal values depending on the dimensionality of the system, t' may be found in a wider range of values and obeys the following relationship [5]:

$$t' = m_h \Phi_c = m_l (1 - \Phi_c) = \frac{m_l m_h}{m_l + m_h} \tag{7}$$

Equation 7 holds if the two phases of the binary system are randomly oriented spheroids, i.e., ellipsoidal grains having semiaxes $a = b \neq c$; then, the coefficients m_h and m_l satisfy the following equations [8, 19]:

$$\begin{cases} m_h = \dfrac{1 + 3L_h^c}{3L_h^c\left(1 - L_h^c\right)} \\ m_l = \dfrac{5 - 3L_l^c}{3\left(1 - L_l^{c^2}\right)} \end{cases} . \tag{8}$$

$L_{h(l)}^c$ denote the effective depolarisation factors of the high- (low-) conductivity phases associated with the principal axis (c) of the ellipsoids, and are directly linked to the shape of the grains. Indeed, the eccentricity e of the ellipsoids and their corresponding depolarisation factors L^c are written as [20]:

prolate ellipsoids ($a/c < 1$):

$$\begin{cases} e = \sqrt{1 - (a/c)^2} \\ L^c = \dfrac{1 - e^2}{2e^3} \left[\ln\left(\dfrac{1 + e}{1 - e} \right) - 2e \right] \end{cases} \tag{9a}$$

oblate ellipsoids ($a/c > 1$):

$$\begin{cases} e = \sqrt{(a/c)^2 - 1} \\ L^c = \dfrac{1 + e^2}{e^3} \left[e - \arctan e \right] \end{cases} \tag{9b}$$

In each case, if $a = b = c$, i.e., corresponding to spherical grains, then $e \to 0$ and $L^c \to 1/3$. Then, according to Equation 8, m_h and m_l take their minimum values 3 and 3/2, respectively. If the aspect ratio a/c vanishes, i.e., corresponding to fibres or needles, then $L^c \to 0$. Therefore, $m_h \to \infty$ while $m_l \to 5/3$. Conversely, $L^c \to 1$ for high values of a/c, i.e., corresponding to thin discs. Hence, for such a morphology, both m_h and m_l tend to infinity.

Fitting the conductivity measurements to either Equation 3 or 6 is not straightforward, since three adjustable parameters are simultaneously implied and, moreover, the critical exponents are strongly sensitive to the position of the threshold [21–25]. For that reason, the fits were carried out by fixing the value of Φ_c. Just like in other works [8–10] for which very relevant results were obtained, Φ_c was estimated from the apparent density of the constituting grains arranged in a loose packing. Indeed, for a number of materials, the percolation threshold was found to be slightly smaller than the packing fraction Φ_p of the percolating particles [26]. The correlation between Φ_c and Φ_p is presented in Fig. 4, and such data were fitted by a second-order polynomial. The value of Φ_c thus corresponding to the measured $\Phi_p = d_p/d_{wf} \approx 6.85 \times 10^{-2}$ was found to be $\Phi_c \approx 6.14 \times 10^{-2}$. Such a

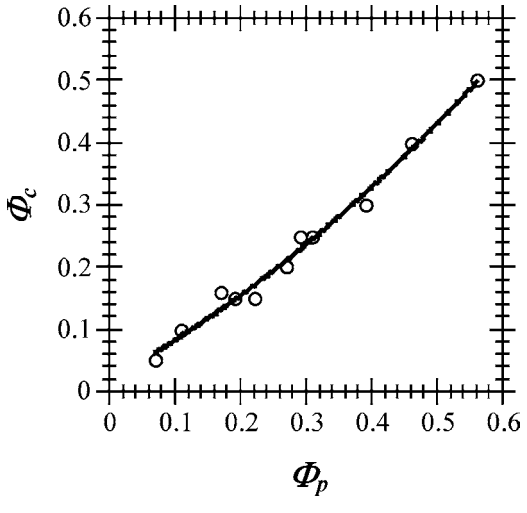

Figure 4 Experimental correlation (for a number of different powdery materials) between percolation thresholds Φ_c, expressed as critical volume fractions of particles, and packing fractions Φ_p of the same particles (after [26]). The solid curve is a second-order polynomial fit to the experimental data points.

TABLE I Parameters m and depolarisation factors L^c derived from the fit of Equation 6 to the conductivity data of Fig. 3. The carbon particles correspond the high-conductivity phase (subscript h in Equation 8) while the interparticle voids are the low-conductivity phase (subscript l in Equation 8). a/c is the aspect ratio of each phase, being either lower than 1 for prolate (i.e., elongated) spheroids, or greater than 1 for oblate (i.e., flattened) spheroids

	Carbon particles	Interparticle voids
m	23.31	1.52
L^c	1.518×10^{-2}	4.37×10^{-1} (oblate) or 2.21×10^{-1} (prolate)
a/c	8.29×10^{-2}	1.45 (oblate) or 6.33×10^{-1} (prolate)

critical volume fraction corresponds to a critical density $d_c = \Phi_c \times d_{wf} \approx 8.53 \times 10^{-2}$ g cm^{-3}.

Equation 6 was fitted to the conductivity data on the whole range of composition, see Fig. 3, using the above fixed value of Φ_c. The fitted curve is very satisfactory and leads to the following parameters: $\sigma_h \approx 82.7$ S cm^{-1} and $t' \approx 1.431$. The value of σ_h is typical of carbonised wood-based materials (see [9] for examples), while the morphologies of both kinds of "grains" (conducting and isolating) may be derived from t' and Φ_c through Equations 7–9. The values of the parameters m_h, m_l, L_h^c, L_l^c, and the corresponding values of the aspect ratios a/c of each phase are gathered in Table I.

The aspect ratio of the carbon particles corresponds to a ratio length to diameter of $1/(8.29 \times 10^{-2}) \approx 12.06$. Such a value is in good agreement with what was estimated from SEM observations in the previous section of this paper. Concerning the shape of the interparticle spaces, it may be seen that m_l is very close to its minimum value of 3/2, thus corresponding to spherical voids. Indeed, whether the pore phase be oblate or prolate, an aspect ratio close to 1 is derived, see Table I.

This latter finding allows the aspect ratio of the solid grains to be directly derived from the apparent density of the carbon powder. Indeed, if the interparticle voids are spherical, it was shown that [8]:

$$\Phi_c = \frac{9L_h^c(1 - L_h^c)}{2 + L_h^c(15 - 9L_h^c)}. \quad (10)$$

Equation 10 was derived from the symmetric Bruggeman model of EMT, and was already shown to lead to very good results for a number of powders and composite materials [8, 9]. Putting $\Phi_c \approx 6.14 \times 10^{-2}$ in (10), one finds $L_h^c \approx 1.544 \times 10^{-2}$ and hence, through (9a), $a/c \approx 8.32 \times 10^{-2}$. The latter value corresponds to a ratio length to diameter of $1/(8.32 \times 10^{-2}) \approx 12.02$, very close to that, 12.06, found above.

PT may be invoked to support both the value of the percolation threshold and that of the aspect ratio of the carbon particles. Indeed, Equation 3 may be applied only very close to Φ_c and, as shown in Fig. 5, the exponent is found to be $t \approx 1.81$: this value is in excellent agreement with what was expected in these three-dimensional randomly disordered materials. Finally, basing again on PT, the aspect ratio of the fibre-like particles may be confirmed in a independent way. The excluded volume concept [27] indeed allows to derive lower and upper bounds for the critical volume

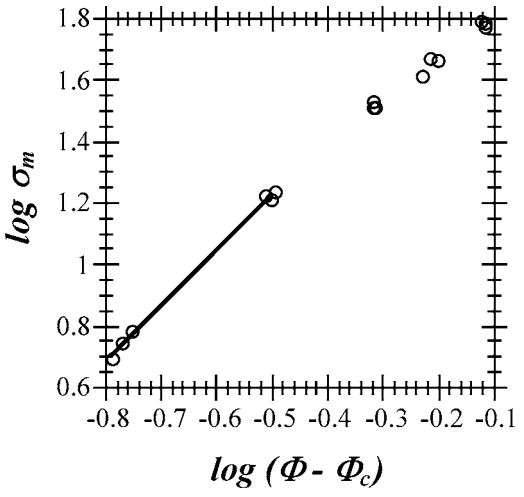

Figure 5 Checking of the percolation conductivity law, Equation 3, near the percolation threshold Φ_c. The critical exponent $t \approx 1.81$ is the slope of the straight line, which holds only in a narrow critical region very close to Φ_c.

fraction of randomly dispersed grains. The excluded volume V_e of a given object is the volume around the latter into which the centre of another similarly shaped objet brought in contact can not penetrate. In the case of percolating cylinders, the percolation threshold is linked to V_e according to Equation 11:

$$1 - \exp\left(-\frac{1.4V}{V_e}\right) \leq \Phi_c \leq 1 - \exp\left(-\frac{2.8V}{V_e}\right), \quad (11)$$

where V is the volume of the percolating grain, and the constants 1.4 and 2.8 are dimensionless invariants corresponding to randomly oriented infinitely thin rods and deformable spheres, respectively [6, 27]. Since the carbon particles may be seen as thick rods, such a morphology being thus intermediate between infinitely thin rods and spheres, the actual value of Φ_c is bounded by these two limits given in Equation 11. If capped cylinders are considered, i.e., cylinders of length L and diameter W comprising at each end a half sphere of radius $W/2$, the volume and the excluded volume read [6]:

$$\begin{cases} V = (\pi/4)W^2L + (\pi/6)W^3 \\ V_e = (4\pi/3)W^3 + 2\pi W^2L + (\pi/2)WL^2 \end{cases} \quad (12)$$

The ratio length to diameter of the fibres was estimated above to be close to 12; putting $L = 12$ and $W = 1$ in Equations 11–12, one gets:

$$4.45 \times 10^{-2} \leq \Phi_c \leq 8.71 \times 10^{-2}, \quad (13)$$

in very good agreement with the previous findings.

3.2. Elastic moduli

Elastic moduli of the wood-based carbon materials were determined for samples of the size $6 \times 10 \times 60$ mm by three point bending tests according to the german industrial standard DIN 51902. Eight samples per density range were tested with a universal testing apparatus (TesT 112.50 $kn.L$) at room temperature.

While randomly disordered, but initially isolated, particles are forced to come closer to each other, two percolation transitions are crossed. The first one, investigated above, corresponds to the inset of a connected path all through the system. The connectivity threshold Φ_c is just below the packing fraction and, at that critical point, the system is not consolidated. The density of the packing thus needs to be higher for the particles to form a rigid network. The critical volume fraction at which the elastic modulus becomes non-zero for the first time is called the rigidity threshold, Φ_r. Hence, in such a particulate system, it is obvious that $\Phi_r > \Phi_c$, while the situation $\Phi_r = \Phi_c$ may be encountered in continuous randomly depleted systems. Anyway, above but close to Φ_r, the elastic modulus is expected to follow the percolation scaling law [3]:

$$E = E_0(\Phi - \Phi_r)^\tau, \tag{14}$$

where E_0 is the elastic modulus at zero porosity and τ is the critical exponent for elasticity. Such a behaviour is known for many heterogeneous media, and especially for sintered materials [28, 29]. Just like t, τ is universal, however its value also depends on the nature of the elastic forces acting between the contacting particles. If central forces (i.e., normal to the surface of the particles, like in most granular systems) prevail, $\tau \approx t$ in three-dimensional media, while $\tau \approx 2t$ if beam-like or angular forces control the elastic behaviour [30–36]. Note that the situation $\Phi_r > \Phi_c$ is a common feature of systems in which central forces prevail over any other kind of elastic forces.

Monolithic compressed expanded graphite is another material in which the two percolation transitions, such that $\Phi_r > \Phi_c$, are met [37]. However, in contrast with the present monoliths, the consolidated blocks that can be prepared from expanded graphite do not need the presence of a binder, since the particles self interlock into each other. To our opinion, since the binder is randomly dispersed among the fibre-like particles, its presence should not influence the position of the rigidity threshold. In other words, adding the phenolic resin should just make the particles sticky, and a previous study indeed showed that various amounts of binder had only a low influence on the apparent density of the blocks [38].

Concerning compressed expanded graphite, the following relationship was evidenced for three different batches of particles [12, 39]:

$$\frac{\Phi_r}{\Phi_c} = \frac{8}{5}. \tag{15}$$

Equation 15 was justified theoretically [12] on the basis of the so-called Kirkwood-Keating model [3 and ref. therein], for which central forces are prevalent but not strictly alone. A few other elastic forces are necessary to account for the rather low rigidity threshold, i.e., only 1.6 times larger than the connectivity one according to Equation 15. Indeed, if the forces were purely central, one should have $\Phi_r = 2(D-1)\Phi_c$, D being the dimensionality of the system [12 and ref. therein],

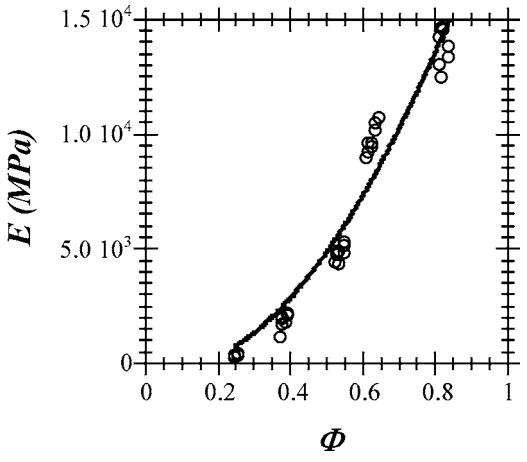

Figure 6 Elastic modulus (E) of the wood-based monoliths as a function of their volume fraction (Φ) of carbon particles. The solid curve is the fit of the PT-derived Equation 14 to the experimental data points.

and hence $\Phi_r = 4\Phi_c$ if $D = 3$. Applying this latter formula to the present monoliths leads to a rigidity threshold of 0.2455, thus corresponding to a critical density of 0.341 g cm^{-3}. Now, the lowest density investigated here, and for which the monoliths are still well consolidated, is lower: 0.3 g cm^{-3}. It is then clear that the elastic forces can not be purely central.

If Equation 15 applies to the present monolithic materials, then $\Phi_r = 1.6 \times \Phi_c \approx 9.82 \times 10^{-2}$. Using this latter value, the percolation law (14) was fitted to the elasticity data, see Fig. 6. The agreement between the experimental points and the calculated curve is satisfactory, and the obtained values for E_0 and τ are 26.2×10^3 MPa and 1.83, respectively. E_0 is in the same order of magnitude than what is usually found for a number of non porous carbonaceous materials [11, 40], while the elasticity exponent is almost equal to the conductivity one, thus strongly supporting the prevalence of central forces within the monoliths. However, a few other kinds of forces (e.g., angular) are required and enough to lower dramatically the rigidity threshold without affecting the value of the critical exponent. Such a description of the material matches the Kirkwood-Keating model which predicts Equation 15. While such a model was already confirmed by numerical simulations [41], it is to our knowledge only the second time that it applies to a real three-dimensional material. Finally, it may be noticed that the universal value of the exponent τ was obtained from the data points corresponding to the whole range of densities, while the universal value of t was observed only very close to Φ_c. Surprisingly, a critical region for the elastic modulus much wider than that of the electrical conductivity was also evidenced in the case of compressed expanded graphite [10, 11, 39].

4. Conclusions

In this work, some physical properties of new carbon porous monoliths were investigated. Using cheap materials, i.e., wood fibres and a few phenolic resin, consolidated blocks having porosities ranging from 40 to 85% could be obtained through a simple process. They are characterised by good electrical

conductivities, although typical of heat-treated carbons ($\approx$10–60 S cm^{-1}). Such satisfactory conducting properties allow these materials to be used as porous electrodes and light electromagnetic shields [42]. Besides, once activated, such carbons should behave as adsorbents having electrical and thermal conductivities both much greater than those of classical granular adsorbent beds; such a feature could be very interesting both for the adsorption process itself, which is exothermal, and for the regeneration of the adsorbent. Additionally, monoliths are more easily handled than powders. Finally, dispersing small catalytic particles onto such conducting high-area rigid supports should be worth studied.

From a more academic point of view, typical percolation behaviours were evidenced in such randomly disordered materials, still prolonging the extensive list of systems to which percolation theory applies. Effective-medium theory was also shown to be a useful complementary tool, enabling the accurate determination of the aspect ratios of the constituting grains and those of the interparticle voids. Finding the signature of central elastic forces through the value of the corresponding critical exponent on the one hand, and observing the relationship $\Phi_r = 8/5\Phi_c$ between the two critical points on the other hand, supported the relevance of the Kirkwood-Keating model. So far, the latter was only found to apply to compressed expanded graphite.

It thus seems that disordered carbon materials are really accurately described by the classical concepts of disordered matter physics (critical phenomena, excluded volume, average coordination of dispersed objects, ...), and thus are good candidates for testing a number of modern theories.

Acknowledgements

The authors are indebted to Nathalie Job, from the LGC of the Liège University (Belgium), for carrying out the measurements of surface area and pore texture of the carbonised wood fibres. Financial support for this research came from the Deutsche Forschungsgemeinschaft (DFG).

References

1. M. SAHIMI, in "Applications of Percolation Theory" (Taylor and Francis, Bristol, PA, 1994).
2. M. SAHIMI, *Rev. Mod. Phys*. **65** (1993) 1393.
3. *Idem.*, *Phys. Rep*. **306** (1998) 213.
4. R. LANDAUER, in AIP Conference Proceedings No 40: Electrical Transport and Optical Properties of Inhomogeneous Media, edited by J. C. Garland and D. B. Tanner (American Institute of Physics, New-York, 1978) p. 2.
5. D. S. MCLACHLAN, M. BLASZKIEWICZ and R. E. NEWNHAM, *J. Amer. Ceram. Soc*. **73** (1990) 2187.
6. A. CELZARD, E. MCRAE, C. DELEUZE, M. DUFORT, G. FURDIN and J. F. MARÊCHÉ, *Phys. Rev. B* **53** (1996) 6209.
7. A. CELZARD, J. F. MARÊCHÉ, F. PAYOT, D. BÉGIN and G. FURDIN, *Carbon* **38** (2000) 1207.
8. A. CELZARD, J. F. MARÊCHÉ and F. PAYOT, *J. Phys. D: Appl. Phys*. **33** (2000) 1556.
9. A. CELZARD, J. F. MARÊCHÉ, F. PAYOT and G. FURDIN, *Carbon* **40** (2002) 2801.
10. A. CELZARD, J. F. MARÊCHÉ, G. FURDIN and S. PURICELLI, *J. Phys. D: Appl. Phys*. **33** (2000) 3094.
11. M. KRZESIÑSKA, A. CELZARD, J. F. MARÊCHÉ and S. PURICELLI, *J. Mater. Res*. **16** (2001) 606.
12. A. CELZARD, M. KRZESIÑSKA, J. F. MARÊCHÉ and S. PURICELLI, *Physica A* **294** (2001) 283.
13. A. CELZARD, J. F. MARÊCHÉ and G. FURDIN, *J. Phys.: Condens. Matter* **15** (2003) 7213.
14. R. FISCH and A. BROOKS HARRIS, *Phys. Rev. B* **18** (1978) 416.
15. D. S. McLACHLAN, *J. Phys. C: Solid St. Phys*. **19** (1986) 1339.
16. *Idem.*, *ibid*. **20** (1987) 865.
17. M. A. J. MICHELS, *J. Phys.: Condens. Matter* **4** (1992) 3961.
18. D. S. McLACHLAN, in Mater. Res. Soc. Symp. Proc. (Symposium Mater. Res. Soc., Pittsburgh, PA, 1996) Vol. 411, p. 309.
19. R. E. MEREDITH and C. W. TOBIAS, *Adv. Electrochem. Electrochem. Eng*. **2** (1962) 15.
20. L. D. LANDAU and E. M. LIFSHITZ, in "Electrodynamic of Continuous Media" (Pergamon, New York, 1980).
21. S. FENG and P. N. SEN, *Phys. Rev. Lett*. **52** (1984) 216.
22. A. HANSEN and S. ROUX, *Phys. Rev. B* **40** (1989) 749.
23. D. J. BERGMAN, *Phys. Rev. B* **31** (1985) 1696.
24. S. ROUX and A. HANSEN, *Europhys. Lett.* **6** (1988) 301.
25. A. HANSEN and S. ROUX, *J. Stat. Phys*. **53** (1988) 759.
26. G. R. RUSCHAU and R.E. NEWNHAM, *J. Compos. Mater*. **26** (1992) 2727.
27. I. BALBERG, C. H. ANDERSON, S. ALEXANDER and N. WAGNER, *Phys. Rev. B* **30** (1984) 3933.
28. C. W. NAN and D. M. SMITH, *Mater. Sci. Eng. B* **10** (1991) 99.
29. N. DEPREZ, D. S. MCLACHLAN and I. SIGALAS, *Solid State Commun*. **66** (1988) 869.
30. M. SAHIMI and S. ARBABI, *Phys. Rev. B* **47** (1993) 703.
31. S. ROUX, *C. R. Acad. Sci. (Sér. 2)* **301** (1985) 367.
32. Y. KANTOR and I. WEBMAN, *Phys. Rev. Lett*. **52** (1984) 1891.
33. S. ROUX, *J. Phys. A, Math. Gen.* **19** (1986) L351.
34. E. DEL GADO, L. DE ARCANGELIS and A. CONIGLIO, *Europhys. Lett.* **46** (1999) 288.
35. M. SAHIMI, *J. Phys. C: Solid State Phys*. **19** (1986) L79.
36. S. FENG, P.N. SEN, B.I. HALPERIN and C. J. LOBB, *Phys. Rev. B* **30** (1984) 5386.
37. A. CELZARD, S. SCHNEIDER and J. F. MARÊCHÉ, *Carbon* **40** (2002) 2185.
38. O. TREUSCH, A. HOFENAUER, F. TRÖGER, J. FROMM and G. WEGENER, in Proceedings of the International Conference on Carbon: Carbon'03, Oviedo, Spain, July 2003, edited by A. Linares-Solano and D. Cazorla-Amorós (The Spanish Carbon Group, Alicante, 2003) p.46 .
39. A. CELZARD, J. F. MARÊCHÉ and G. FURDIN, *Prog. Mater. Sci*. **50** (2005) 93.
40. GROUPE FRANÇAIS D'ETUDE DES CARBONES, "Les Carbones" (Masson, Paris, 1965).
41. H. HE and M. F. THORPE, *Phys. Rev. Lett*. **54** (1985) 2107.
42. T. OKABE, K. SAITO and K. HOKKIRIGAWA, *J. Porous Mater*. **2** (1996) 207.

Received 8 March
and accepted 31 August 2004